Domain wall propagation in ferromagnetic semiconductors: Beyond the one-dimensional model

L. Thevenard,[1,*] C. Gourdon,[1] S. Haghgoo,[1] J-P. Adam,[2] H. J. von Bardeleben,[1] A. Lemaître,[3] W. Schoch,[4] and A. Thiaville[2]

[1]*Institut des Nanosciences de Paris, Université Pierre et Marie Curie, CNRS, UMR 7588, 4 place Jussieu,75252 Paris, France*
[2]*Laboratoire de Physique des Solides, CNRS - Université Paris-Sud, bât. 510, 91405 Orsay, France*
[3]*Laboratoire de Photonique et Nanostructures, CNRS, UPR 20, Route de Nozay, Marcoussis, 91460, France*
[4]*Institut für Quantenmaterie, Universität Ulm, 89069 Ulm, Germany*

We have investigated experimentally the field-driven propagation of domain walls (DWs) in perpendicularly magnetized ferromagnetic semiconductor layers. The results were then compared with the historical one-dimensional (1D) DW propagation model widely used in spintronics studies of magnetic nanostructures. Anomalous velocity peaks, not predicted by the 1D model, were observed experimentally. Using micromagnetic simulations we show indeed that, in the particular regime of layer thickness (h) of the order of the exchange length, velocity peaks appear in the precessional regime, their shape and position shifting with h. Analyses of the simulations show a distinct correlation between the curvature of the DW and the twist of the magnetization vector within it and the velocity peak. Associating a phenomenological description of this twist with a four-coordinate DW propagation model, we show that the velocity peaks result from the torque exerted by the stray field created by the domains on the twisted magnetization. The position of the peaks is well predicted from the DW's first flexural mode frequency and depends strongly on the layer thickness. Comparison of the proposed model with data obtained on GaMnAs and GaMnAsP shows that the anomalies observed close to Walker breakdown are indeed induced by the flexion resonance of the domain wall.

I. INTRODUCTION

The 1970s saw the establishment of the main theories describing magnetic domain wall (DW) propagation, among which is the so-called one-dimensional (1D) model.[1–5] These studies fueled the intense efforts toward the building of magnetic bubble memories. They have recently come back into fashion, with new schemes being proposed to use domains or DWs as the building blocks of a nonvolatile and downscalable memory.[6–8] Described in different formalisms,[1–5] the 1D model assumes that the DW propagation can be fully described by two time-dependent variables: the position $q_0(t)$ of the DW and the azimuthal angle $\phi_0(t)$ of the magnetization unit vector $\vec{m}$ inside the DW. For a defect-free sample, the velocity versus field curve v(H) is then shown to consist of a high-mobility regime where the configuration of $\vec{m}$ within the DW is stationary [$\phi_0(t)$ constant] up to the Walker field H_W, followed by a negative-mobility regime and then again a linear, lower-mobility regime, where $\vec{m}$ precesses around the applied field.

While these two regimes have indeed been evidenced experimentally,[9–11] one or two unexpected kinks have repeatedly been observed in a variety of configurations: in-plane magnetized Permalloy,[12,13] out-of-plane magnetized garnets,[14] as well as out-of-plane magnetized ferromagnetic semiconductor GaMnAs.[10] It has also been observed in field-assisted current-induced propagation.[15] The present paper aims to address this issue, all the more crucial as the 1D model is now routinely used as a guideline for a vast number of studies on current-induced DW propagation.[16–18] Whereas differences with the 1D model in the stationary regime were attributed quite early on to the nucleation/annihilation of Bloch lines,[19] those in the precessional regimes have been considered only by the numerical simulations of Patterson *et al.*[20] (perpendicularly magnetized layer), who did not isolate

the physical mechanism(s) for these kinks. A very recent paper has investigated this phenomenon in in-plane magnetized layers.[13]

In the following section of this paper (Sec. II), we present experimental v(H) curves obtained on perpendicularly magnetized GaMnAs and GaMnAsP thin films of varying thickness, magnetization, magnetic anisotropy, and exchange constant. Ferromagnetic semiconductors offer weak pinning which conveniently allows all DW propagation regimes to be observed.[10] Their magnetic parameters can easily be tuned by careful doping[21–23] or by varying the temperature. The layer thickness can also be varied across the exchange length. In both of these materials we obtained an unusual velocity versus field behavior, which we then investigated numerically. In Sec. III, we present simulated v(H) curves for perpendicularly magnetized ferromagnetic layers of increasing thickness ($h = 10$–40 nm) obtained with an open source micromagnetic simulation software[24] in the (2D) two dimensional limit. In Sec. IV, we analyze extensively the three-component magnetic configuration within the DWs and relate it to the position of the v(H) peaks in Sec. V. In particular, we give evidence on the role of the flexion of the DW and the twist of its magnetization vector in increasing the DW velocity above the 1D model value for certain fields. Those particular fields are found to correspond to the first flexural mode resonance of the DW. Section VI compares these findings with the experimental data and discusses how they can relate to DW propagation in other geometries.

II. EXPERIMENTAL RESULTS

Figure 1 summarizes the experimental results obtained on out-of-plane magnetized GaMnAs and GaMnAsP layers. In all these measurements, the DW velocity was determined using

magneto-optical imaging and a magnetic field pulse technique fully described in Ref. 10. Figure 1(a) shows the v(H) curve at 20, 50, and 80 K for a 50-nm-thick $Ga_{0.93}Mn_{0.08}As_{0.915}P_{0.085}$ layer grown over GaAs. Figure 1(b),1(c), and 1(d) show data for three $Ga_{0.93}Mn_{0.07}As$ samples grown on an $In_yGa_{1-y}As$ pseudo-substrate: $h = 50$ nm at temperatures 4–90 K ($y = 10\%$, previously published in Ref. 10), $h = 20$ nm ($y = 15\%$, T = 40 K) and $h = 40$ nm ($y = 15\%$, T = 60 K). After annealing, these last two layers have Curie temperatures of, respectively, 118 K and 136 K. The micromagnetic parameters of both $h = 50$ nm layers were determined using Kerr microscopy as detailed in Ref. 21 (where they are referred to as samples B and D). The main differences between these two samples are a higher uniaxial anisotropy in GaMnAs and a higher exchange constant and saturation magnetization in GaMnAsP.

All the v(H) curves roughly follow the 1D model: They exhibit a high mobility up to the Walker field (5–7 mT), followed at high fields by a lower mobility in the precessional regime. However, they also evidence anomalies with respect to the 1D model curve in two regions broadly indicated by polygons in Fig. 1. At low fields in the precessional regime (region 1), the velocity is almost constant instead of decreasing, as expected from the 1D model. At low temperatures, the $h = 50$ nm GaMnAs and GaMnAsP curves all show a plateau in velocity which is progressively pushed downward toward the Walker peak as the temperature is increased. At T $=80$–90 K, a negative-mobility region is eventually obtained. The $h = 40$ nm curve shows a broad kink around Walker breakdown ($\mu_0 H_W \approx 5$ mT), while the $h = 20$ nm curve exhibits distinctly Walker breakdown ($\mu_0 H_W = 14$ mT), a narrow negative mobility region before a kink at 23 mT. At higher fields (region 2), kinks of varying amplitude appear.

In the GaMnAs data [Figs. 1(b)–1(d)], the $h = 50$ nm curves show a weakly temperature-dependent kink at around 100–110 mT, the $h = 40$ nm a split kink centered around 100 mT, and the $h = 20$ nm once again a broad split kink centered around 105 mT. The GaMnAsP curve [Fig. 1(a)] also exhibits a very broad bump appearing in region 2: around 50 mT at T = 20, 50 K, and 34 mT at T = 80 K. To summarize, all samples exhibit a broad, high-field kink (region 2) whose position varies weakly with the layer's thickness and magnetization (temperature), and a low-field feature (region 1) that shifts downward with temperature and thickness.

III. SIMULATIONS

A. Geometry and results

To identify the physical origins of these peaks, numerical simulations were performed varying only one parameter in the first place: the thickness of the layer. The film was taken as infinite in the x direction, as shown in Fig. 2(a). The DW propagates along the y direction. The normal to the film is denoted z. The simulation was laid out on a 2D mesh with cell dimensions c^2, and a strip of length[25] $d = 1\,\mu$m. The FastPipe magnetostatic calculation procedure was used. The thicknesses investigated were $h = 10$ nm ($c = 1$ nm), and $h = 20, 30, 40$ nm ($c = 2$ nm). The applied field $H = H_z$ was constant and perpendicular to the plane of the layer, and micromagnetic parameters typical of GaMnAs at T = 80 K[10,26] were used: magnetization $M = 33$ kA m^{-1}, uniaxial anisotropy coefficient $K_u = 8878$ J m^{-3} and field $\mu_0 H_u = 2K_u/M$, and exchange constant $A = 5.10^{-14}$ J m^{-1}. The resulting exchange length was $\Lambda = \sqrt{2A/\mu_0 M^2} = 8.6$ nm, i.e., of the order of h. Given the high value of the factor $Q = \frac{2K_u}{\mu_0 M^2} > 3$ in our layers, the complex in-plane anisotropy of GaMnAs was
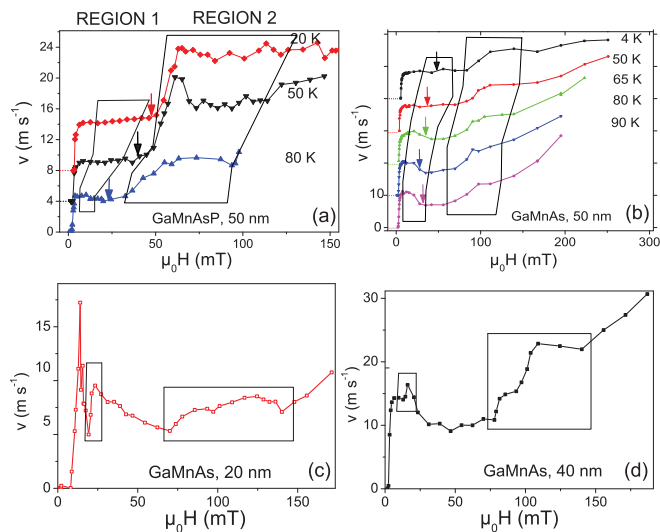

FIG. 1. (Color online) Experimental velocity versus field data (curves shifted for clarity where needed). The polygons indicate the velocity anomaly regions, labeled 1 (low field) and 2 (high field). The arrows point to the $H = 0$ resonance fields of the DW flexural modes determined numerically (see Section VI). (a) $Ga_{0.93}Mn_{0.08}As_{0.0915}P_{0.085}$, $h = 50$ nm. (b) $Ga_{0.93}Mn_{0.07}As$, $h = 50$ nm (reproduced from Ref. 10). (c) $Ga_{0.93}Mn_{0.07}As$, $h = 20$ nm. (T = 40 K), (d) $h = 40$ nm (T = 60 K).
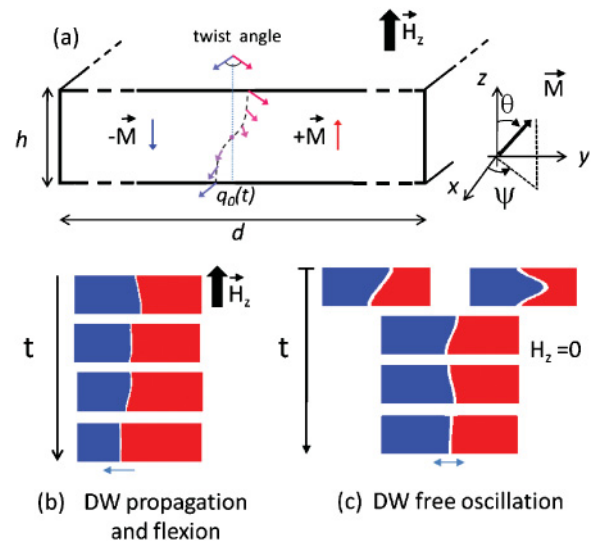

FIG. 2. (Color online) (a) Geometry of the simulation, side view of the layer. The DW propagates toward the left; its mean position along y is given by q_0(t) (not to scale). (b) DW propagation evidencing curvature, shown here for $h = 80$ nm to highlight the effect. (c) DW free oscillation ($H_z = 0$), after initializing the simulation from either of the top two positions. Magnetic parameters used for the simulations are indicated in the text.

ignored. Its influence will be discussed later. The damping coefficient was taken as $\alpha = 0.3$. This rather large damping coefficient was determined self-consistently using DW dynamics measurements[10] and is about an order of magnitude higher than that found by ferromagnetic resonance[27] (FMR). As explained in greater details in Ref. [10], this discrepancy was already encountered in garnets, and mainly stems from the fact that dissipation phenomena largely differ for a moving DW (the present study and Ref. [10]) or a uniform magnetization (FMR studies).

The magnetization orientation vector $\vec{m}$ is three dimensional (3D), but laid out on a 2D mesh. It was defined in Cartesian $(m_x, m_y, m_z)(y,z)$ coordinates. Within the domain wall, we used the standard $(q, \theta, \psi)(z,t)$ coordinates [Fig. 2(a)], where $q(z,t)$ denotes the position of the DW along the propagation direction, θ is the polar angle of the magnetization in the DW with respect to the film normal, and ψ is the azimuthal angle with respect to the x axis. Averaging over z yields the usual coordinates $(q_0, \Theta, \phi)(t)$ with the well-known relationship $\dot{\Theta} = -\frac{\dot{q}_0}{\Delta} \sin \Theta$, where the dot denotes the time derivative[5] and $\Delta = \sqrt{A/K}$ is the static DW width. From the simulations, the instantaneous velocity $\mathrm{v_{inst}} = \frac{d}{2} \frac{\partial \langle m_z \rangle}{\partial t}$ was averaged over many periods, and the resulting v(H) curves are shown in Fig. 3. For comparison, the baseline of the curves was fitted to the 1D model velocity (keeping α fixed to 0.3, and varying $\mu_0 H_W$ and Δ), using the $(q_0, \phi_0)(t)$ solutions to the Landau–Lifshitz–Gilbert (LLG) equation[1] for $H > H_W$:

$$\dot{q}_0(t) = \frac{\gamma \Delta \mu_0 M}{2(1 + \alpha^2)} \sin 2\phi_0 + \frac{\alpha \gamma \Delta}{1 + \alpha^2} \mu_0 H, \quad (1)$$

$$\phi_0(t) = \arctan \left[\frac{H_W}{H} + \sqrt{1 - \left[\frac{H_W}{H} \right]^2} \tan \left(\frac{2\pi t}{T} \right) \right]. \quad (2)$$

In these expressions, $H_W = \alpha M/2$ is the Walker field for a film of infinite thickness and $T = \frac{1 + \alpha^2}{\mu_0 \gamma} \frac{2\pi}{\sqrt{H^2 - H_W^2}}$ is the precession period [time for $\phi_0(t)$ to span $360°$]. The average DW velocity then reads v(H) $= \frac{1}{T} \int_{t=0}^{T} \dot{q}_0(t) dt$.

The simulations were performed up to 300 mT (400 mT for $h = 10$ nm), but only the first part of the curve is shown in Fig. 3 as the mobility remains identical for higher fields. Although the simulations do not fully reproduce the experimental data, some also evidence strong variations to the 1D model close to the Walker peak. For $h = 10$ nm [Fig. 3(a)], the numerical simulations reproduce the standard 1D model curve. A high mobility is observed up to the Walker field, then a narrow negative-mobility region-followed by a positive lower-mobility regime. The DW velocity reaches over $30 \, \mathrm{m \, s^{-1}}$ at $\mu_0 H = 250$ mT. No kinks were observed in the 0–400 mT range. The $h = 20$–40 nm curves evidence a similar behavior up to Walker breakdown, but distinctive kinks appear above: at ≈ 70 mT for $h = 20$ nm, ≈ 37 mT for $h = 30$ nm, and at 25 and 35 mT for $h = 40$ nm. The shape of the kinks also evolves with layer thickness, becoming sharper with increasing h, and even splitting in two for the thickest $h = 40$ nm. Walker breakdown occurs at a low field ($\mu_0 H_W = 3$ mT, velocity $V_W = 4 \, \mathrm{ms^{-1}}$) for the thinnest layer, and then gradually converges to the infinite thickness film value $\mu_0 H_W = 6$ mT for $h = 40$ nm. In parallel, Δ decreases slightly with thickness (from 2.6 to
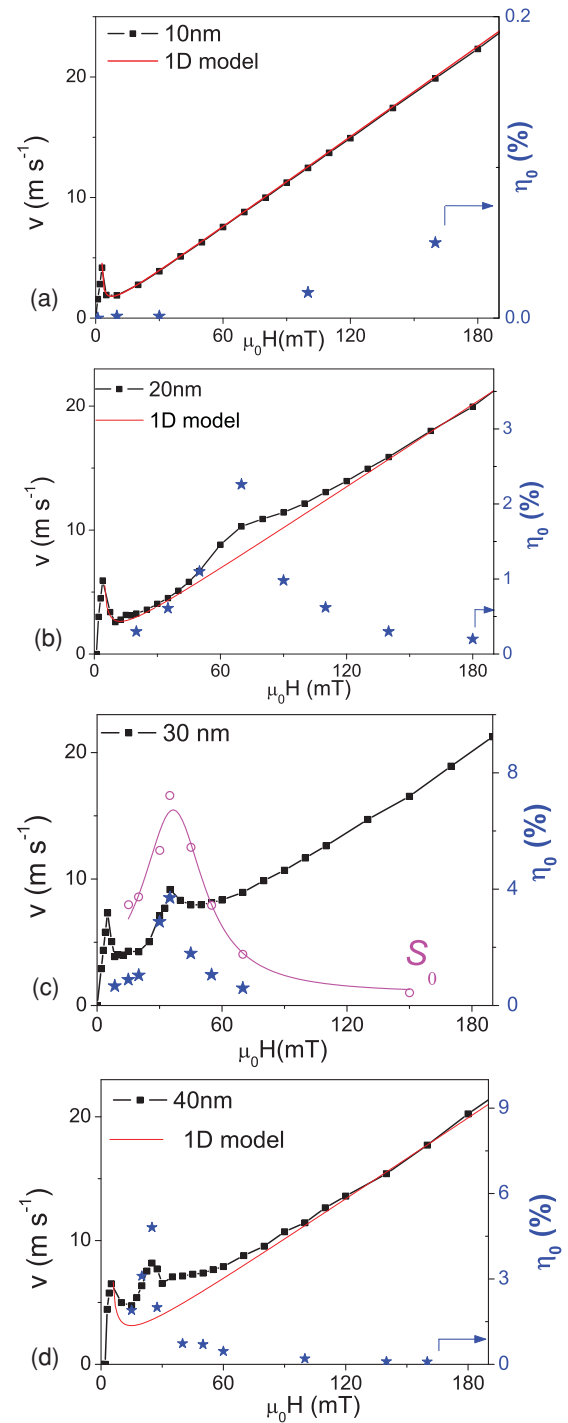

FIG. 3. (Color online) Simulated velocity versus field (squares): (a) $h = 10$ nm, (b) $h = 20$ nm, (c) $h = 30$ nm, and (d) $h = 40$ nm. In (a), (b) and (d), the solid line is a fit to the 1D model, and the stars are the maximum DW elongation η_0. In (c) the open circles are the twist amplitude S_0 and its Lorentzian fit (solid line). Extrema values of the twist are $8°$ and $108°$.

2.3 nm), reflecting the change of demagnetizing factors of the DW with layer thickness, which in turn modifies the values of H_W and Δ.[28] The precession frequency of the magnetization f_{prec} obtained as the inverse of the period of $m_x(t)$ was found identical for all thicknesses and linear with the applied field.

B. Image analysis

The time-dependent magnetization structures [of the type in Figs. 2(b) and 2(c)] were then treated numerically to extract for every 100 iterations the DW width Δ and the depth-dependent DW position $q(z,t)$ and $\psi(z,t)$ angle (the latter averaged over 2Δ along y). The z-averaged angle $\phi(t)$ is given by $\frac{1}{N_i} \sum_1^{N_i} \psi_i(z,t)$ with N_i the number of cells across the thickness. Plotting simultaneously $v_{inst}(t)$ and $\phi(t)$ for $H > H_W$ over one precession period shows the main features of the precessional regime [Fig. 4(a)]: $\vec{m}$ precesses around the applied field, inducing a demagnetizing field across the wall. This sinusoidal field produces a torque on $\vec{m}$, leading to an alternating forward or backward motion of the DW. The applied field term in Eq. (1) ensures that the total wall displacement over one period is strictly positive. As expected from the 1D expression for $\phi_0(t)$ [Eqs. (1), (2)], the instantaneous velocity is then maximum for $\phi = 45°$ (modulo 180°) and minimum for $\Phi = 135°$ [180°], corresponding to the extrema of the demagnetizing torque [arrows in Fig. 4(a)].

Meanwhile, the DW length is not constant but undergoes a T-periodic elongation which shows up as a time-dependent flexion in Figs. 2(b) and 4(b). To quantify this flexion, we define the elongation of the DW as $\eta(t) = [l(t) - h]/h$ where $l(t)$ is the curvilinear integral of $q(z,t)$. The simulations show that the DW goes from no elongation ($l = h$, $\eta = 0$) to the maximum (η_0, stars in Fig. 3) while $\phi(t)$ varies from 0 to 360°. Careful analysis shows that the curvature is always of an $n = 1$ mode type (following the numbering of Slonczewski[29]), i.e., odd about the layer's midheight. For all layers, $\eta_0(H)$ reaches a maximum at a resonance field H_{res} which decreases with increasing layer thickness. This maximum elongation increases with h: $\eta_0 = 1.53\%$ for $h = 10$ nm ($\mu_0 H_{res} = 300$ mT), 2.3% for $h = 20$ nm ($\mu_0 H_{res} = 70$ mT), 3.7% for $h = 30$ nm ($\mu_0 H_{res} = 35$ mT) and 4.8% for $h = 40$ nm ($\mu_0 H_{res} = 25$ mT). Far from H_{res}, the flexion becomes negligible. Note that, setting aside the $h = 10$ nm curve, the H_{res} fields correspond exactly to those of the kinks in the v(H) curve. The enhancement of velocity therefore seems related to the DW flexion.

The depth dependence of the ψ angle of the propagating DW evidences a clear twist of the magnetization from top to bottom of the layer (Fig. 2(a) and 5), but quite differently from the textbook 180° twist case of a static Néel–Bloch–Néel DW.[3,30] Plotting $\psi(z,t)$ over a whole period shows that the twist is sinusoidal across the layer's thickness, and that its amplitude $S(t)$ also varies sinusoidally in time over T with a span of S_0 [Fig. 5(a)]. The time and depth dependence of
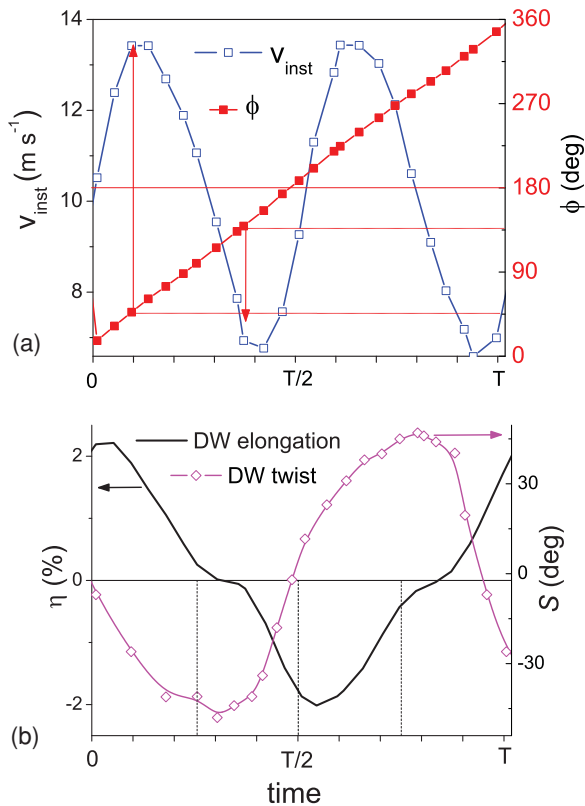

FIG. 4. (Color online) Dynamics over one precession period under $\mu_0 H = 70$ mT for the sample $h = 20$ nm. (a) Instantaneous velocity (open squares) and mean $\phi(t)$ (full squares) over one precession period. Arrows indicate maximum (minimum) velocities for the canting angle close to 45° (modulo 180°) [135° (modulo 180°)]. (b) DW elongation (η, solid line) and DW twist (S, line with diamonds).
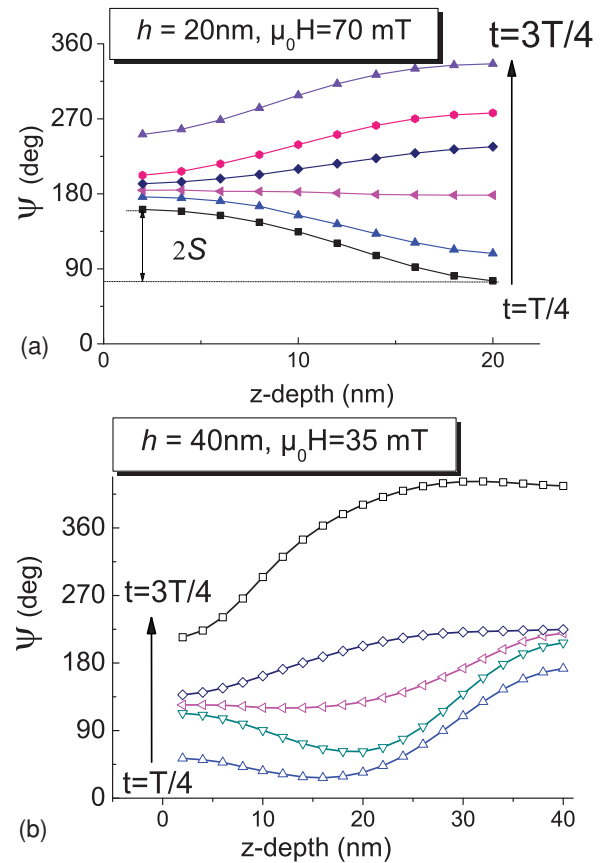

FIG. 5. (Color online) Depth dependence of $\psi(z,t)$ over half a precession period for (a) $h = 20$ nm, $\mu_0 H = 70$ mT and (b) $h = 40$ nm, $\mu_0 H = 35$ mT. Weakly localized horizontal Bloch lines appear in the thicker layer.

$\psi(z,t)$ are then described in the first approximation by the following phenomenological expressions:

$$\psi(z,t) = \phi_0(t) + \tilde{\psi}(z,t), \tag{3}$$

$$\tilde{\psi}(z,t) = -S(t,H)\cos\frac{\pi z}{h}, \tag{4}$$

$$S(t,H) = -S_0(H)\sin\frac{2\pi t}{T(H)}. \tag{5}$$

For $h =$10–30 nm and $h = 40$ nm when $\mu_0 H < 30$ mT, the twist amplitude is minimum for $t = T/4$, maximum around $3T/4$, and null for $t = 0$ (modulo $T/2$) [Fig. 4(b)]. Twist and curvature are intimately related, being in quadrature phase with respect to each other. The thickness dependence of S_0 is as expected: It increases with thickness, since the exchange energy cost of a twist can be more easily accommodated in a thicker layer. Strikingly, $S_0(H)$ follows the same trend as $\eta_0(H)$: It reaches a maximum at $H_{\rm res}$ [see Fig. 3(c) for the $h = 30$ nm case]. At resonance, the full twist amplitude of the DW magnetization across the layer's thickness ($2S_0$) reaches about 90° for $h = 20$ nm, 216° for $h = 30$ nm, and 230° for $h = 40$ nm.

For the thickest layer $h = 40$ nm, a different behavior appears around $\mu_0 H = 30$ mT, as can be seen in Fig. 5(b) : the twisting direction inverts at a given depth. This corresponds to a horizontal Bloch line (HBL). These appear where the magnetization is most labile as a result of the competition between the stray field emanating from the domains and the demagnetizing field within the DW.[3] For $h = 30$ nm, very weakly localized HBLs also appear around 45 mT. This is consistent with the estimated HBL width $\pi \Lambda = 27$ nm. Layers of 30 and 40 nm can thus accommodate with difficulty a full HBL.

To summarize, this first analysis gives two fundamental results: The kinks in the v(H) curves occur at fields maximizing both the curvature and the twist of the DW, and twist and curvature are coupled variables.

IV. ANALYSIS

To get more insight into the respective roles of the DW flexion and magnetization twist on the kinks of the v(H) curves, the analytical model of Malozemoff and Slonczewski[31] will be used. Let us beforehand recall the general equations coupling the time derivatives of $(q_0, \phi_0)(t)$ in the 1D model:

$$\dot{q}_0(t) = \frac{\mu_0 M}{2}\gamma\Delta\sin 2\phi_0 + \alpha\Delta\dot{\phi}_0(t), \tag{6}$$

$$\dot{\phi}_0(t) = -\frac{\alpha\mu_0 M}{2(1+\alpha^2)}\gamma\sin 2\phi_0 + \frac{\gamma}{1+\alpha^2}\mu_0 H. \tag{7}$$

In the precessional regime, the propagation is achieved by a balance of the torque associated with the oscillating demagnetizing field [first term of the right-hand side of Eq. (6)] created by the precession, and the dissipation of the energy brought by the field in the form of a damping contribution (second term). For $H \gg H_W$, the demagnetization term averages out to zero, and the damping term takes over and propels the DW forward with a velocity proportional to the applied field [Eqs. (1),(7)]. In this simple 1D model, two different routes appear to increase v(H): an increased *precession rate* or an increased *damping*.

As mentioned above, however, the simulations showed no substantial difference for $\dot{\phi}$ between the different thicknesses. Concerning the damping, an alternative way for the system to dissipate energy would be by direct coupling to spin waves (SWs) in the bulk of the material, or by a SW-like excitation of the magnetization in the vicinity of the DW.[32,33] Plotting the $m_{x,y,z}(y)$ components for different thicknesses does not evidence any particular wake, but only a slight deformation of the DW profile for $H \approx H_{\rm res}$. Concerning bulk SWs, their lowest ($k = 0$) frequencies[34] lie much higher than the typical precession frequencies, thus forbidding any direct coupling between the DW and bulk SWs. It therefore seems necessary to go beyond the 1D model and take into account the full thickness dependence of the magnetization configuration.

For a twisted DW taken as infinite in the x direction, the DW surface energy is expressed to first order in exchange, magnetostatic, and curvature terms as[31]

$$\sigma = \sigma_0\left[1 + \frac{1}{2}(\nabla q)^2\right] + 2A\Delta(\nabla\psi)^2$$
$$+ \mu_0 M^2\Delta\sin^2\psi - \Delta\mu_0\pi M H_y\sin\psi - 2\mu_0 M H q. \tag{8}$$

In this expression, $\sigma_0 = 4\sqrt{AK}$ is the 1D Bloch wall surface energy. The term $[1 + \frac{1}{2}(\nabla q)^2]$ corresponds to the energy increase due to the elongation of the DW, and the term $A(\nabla\psi)^2$ corresponds to the exchange energy cost arising from the twist. Since q and ϕ are conjugated coordinates, it is reasonable to assume that so are ∇q and $\nabla\psi$. By analogy with a spring or a twisted rope, and looking at Fig. 4(b) , the DW energy contains a kinetic (flexion ∇q) and an elastic (twist $\nabla\psi$) term which balance each other out. When the DW is very twisted, the energy cost of an additional curvature is too high: the flexion is minimal, and vice versa. H_y can stem from volume or surface magnetic charges created by the DW or domains. Here, we will consider only H_y as the y component of the stray field arising from up- and down-domains on either side of the DW. The curvature of the domain will be considered small enough to neglect the fields along y and z resulting from magnetic charges appearing along the DW due to its curvature.[31] Among the different expressions demonstrated for H_y,[3,30] we will use that of Ref. 3, as it remains valid down to the $\Delta \approx h$ limit:

$$4\pi H_y(z) = -2M\ln\left[\frac{z^2 + \Delta^2/4}{(h-z)^2 + \Delta^2/4}\right] + \frac{8M}{\Delta}$$
$$\times\left[z\arctan\left(\frac{\Delta}{2z}\right) - (h-z)\arctan\left(\frac{\Delta}{2(h-z)}\right)\right]. \tag{9}$$

It is determined by computing the potential arising from the $-M$ and $+M$ surface charges (varying linearly over a width Δ) of domains on either side of the DW. Any effects of the volume charges created within the DW are ignored. This field is stationary, but varies throughout the thickness of the material. It pins the magnetization of a static DW in Néel configuration at the surfaces of the layer, so that the equilibrium structure of the wall is twisted. For $h = 30$ nm, it amounts to a field of over 55 mT at the surface of the layer. This is likely an overestimation of the actual H_y though, since
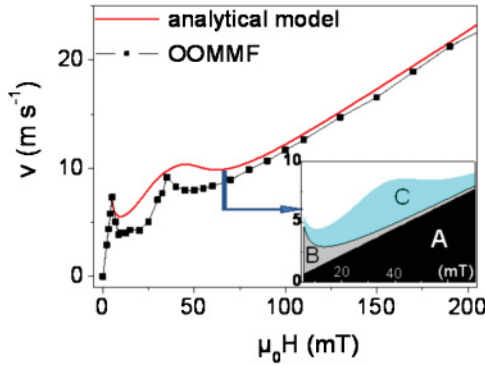
FIG. 6. (Color online) Velocity computed analytically using the $(q, \psi, \nabla q, \nabla \psi)$ model for $h = 30$ nm and $H > H_W$, and the corresponding simulated OOMMF curve. Inset close-up of the kink area evidencing the respective contributions to the velocity of the applied field (A), the demagnetizing field (B), and the domains' stray field (C). See Eq. (10) and text for details.

the volume contribution has been ignored. Finally, using the LLG equation leads to the equation[31]

$$\dot{q}(z,t) = \frac{\gamma \Delta}{1+\alpha^2} \left[\frac{\mu_0 M}{2} \sin 2\psi + \alpha \mu_0 H - \frac{\pi}{2} \mu_0 H_y \cos\psi \right. $$
$$\left. - \frac{2A\nabla^2\psi}{M} + \frac{\alpha\sigma_0\nabla^2 q}{2M} \right]. \quad (10)$$

The DW velocity is then obtained by a double integration on time and space, v(H) = $\frac{1}{T}\int_{t=0}^{T}\frac{1}{h}\int_{z=0}^{h}\dot{q}(z,t)dz\,dt$, provided the canting angle is known. As expressed in Eqs. (3)–(5), $\psi(z,t)$ can easily be written as the sum of the 1D model uniform $\phi_0(t)$ given by Eq. (2), and a depth-dependent angle $\tilde{\psi}(z,t)$ varying sinusoidally across the layer (in the absence of a HBL). Moreover, the oscillation amplitude $S_0(H)$ can be fitted by a Lorentzian [Fig. 3(c) , solid line]. The negative signs in Eqs. (4),(5) mimic the phase seen in the simulations: The twist is null when the wall is in a Bloch configuration ($\phi_0 = 0$ [180°]), and extremum when it is in a pseudo-Néel configuration ($\phi_0 = 90°$ [180°]).

The resulting computed velocity is plotted in Fig. 6 for $h = 30$ nm, along with the corresponding micromagnetic simulation already presented in Fig. 3(c). The Walker field and DW thickness injected in Eq. (10) are those of the 1D model baseline fit of the $h = 30$ nm curve: $\mu_0 H_W = 5$ mT and $\Delta = 2.28$ nm. The v(H) curve obtained using the analytical model given by Eqs. (9) and (10) resembles very much the numerical simulation. The mobility above Walker breakdown is linear for the 1D model curve, but shows a kink when the magnetization twist is taken into account. At the peak ($\mu_0 H \approx 38$ mT), the velocity has increased from 4.7 m s^{-1} to about 10 m s^{-1}, to be compared with the value of 9.2 m s^{-1} obtained in the simulation. At high fields, the calculated curve eventually coincides with the 1D model one. The kink is in fact broader than the one observed in the simulation, which is not surprising considering the approximations needed to establish Eq. (9). A very similar result is obtained for the $h = 20$ nm curve, showing that the velocity increase is due to the twist of the magnetization.

A partial analytical integration of Eq. (10) over t and z gives some insight as to which of the three terms H_y, $\nabla^2 q$, and/or $\nabla^2\psi$– absent from the 1D model expression - governs the shape of v(H). Taking into account the boundary conditions $\frac{\partial\psi}{\partial z}|_{0,h} = \frac{\partial q}{\partial z}|_{0,h} = 0$ immediately shows that the $\nabla^2 q$ and $\nabla^2\psi$ terms do not contribute at all. Using the odd nature about $z = h/2$ of both H_y and $\tilde{\psi}$ then leaves

$$\langle v \rangle = \frac{\Delta\gamma}{1+\alpha^2} \left\{ \frac{\mu_0 M}{2} \frac{1}{T} \int_0^T J_0\left(2S_0 \sin\frac{2\pi t}{T}\right) \sin 2\phi_0 dt \right. $$
$$\left. + \frac{\pi}{2\,Th} \int_0^T \sin\phi_0 \int_0^h \mu_0 H_y(z) \sin\tilde{\psi}\,dzdt + \alpha\,\mu_0 H_z \right\}. $$
$$(11)$$

$J_0(x)$ refers to the $m = 0$ Bessel function of the first kind. In the absence of twist within the DW ($S_0 = 0$), the $\tilde{\psi}$ term vanishes, and the 1D expression is recovered. In the absence of time dependence of the twist [$S(t) = S_0$], the second term in Eq. (11) vanishes by time integration of the T-periodic $\sin\phi_0$ term. This leaves an expression very similar to the 1D equation, save for a decrease by $J_0(2S_0)$ of the demagnetization term.

When the twist is taken to be time dependent as described in Eqs. (3)–(5), the demagnetizing field [first term of Eq. (11)] created across the DW over one period is decreased compared with the pure Bloch DW case, as previously. The second term of Eq. (11) reflects the strength of the torque $\vec{m} \times \vec{H}_y$ averaged over the thickness of the layer, and over a period. Because both the stray field and the z-dependent DW magnetization angle $\tilde{\psi}$ invert signs at midheight of the layer, the integration over the layer thickness of this torque will always be nonzero. The sign of this contribution is moreover given by the phase of the twist amplitude $S(t)$ with respect to the mean azimuthal angle of the DW $\phi_0(t)$. As shown in Fig. 4, when the twist is winding clockwise up the layer ($S < 0$), the magnetization lies opposite the direction of motion ($\phi_0 = 0$–180°, $\sin\phi_0 > 0$). When the twist is winding counterclockwise ($S > 0$), the magnetization is facing the direction of motion ($\phi_0 = 180$–360°, $\sin\phi_0 < 0$). As a result, this integration over a whole precession period yields a net positive contribution to the DW velocity. The amplitude of H_y can easily be of the order of $1.3M$ at the surface, and so the $\vec{m} \times \vec{H}_y$ torque will dominate the first term. Plotting only the applied field and demagnetizing field terms calculated with a twisted magnetization (labeled A and B in the inset Fig. 6) gives a curve very similar to the one computed from the 1D model, Eq. (6). It is thus clearly the stray field term (C) that yields a velocity increase.

For an increased velocity to appear, it is therefore required to combine both a twist of the DW magnetization across the layer, and a particular time dependence of this twist amplitude (negative twist when the mean magnetization angle is in the 0–180° quadrant). As shown above, the twist and curvature are coupled variables. At fields giving a maximum flexion, a maximum twist will therefore also be obtained. The position of the resulting kink in the v(H) curve will then be indirectly related to the field dependence of the curvature $\eta(H)$, given by $\nabla^2 q$. For $h = 10$ nm, the small amplitude of the flexion (and therefore of the twist), and its very broad resonance make the kink undetectable in the v(H) curve.

Finally, we come to the double kink for $h = 40$ nm. At low field the kink is very similar to the $h = 30$ nm curve, but abruptly drops around $\mu_0 H = 30$ mT. Since the velocity increase is directly due to the continuous and symmetrical twist of the DW across the layer's width, HBLs are likely to severely disrupt the scheme presented above, all the more so as the HBL is tighter. As shown in Fig. 5(b), HBLs precisely start appearing around $\mu_0 H = 30$ mT for $h = 40$ nm. They thus seem responsible for splitting the peak into a sharp kink followed by a broad bump.

V. POSITION OF VELOCITY PEAKS

A. Simulations

An important question remains concerning the position of the velocity peaks, as well as their thickness dependence. Because the shape of $\eta_0(H)$ and $S_0(H)$ recalls a resonance, the free oscillation of a DW was investigated. With $H = 0$ in the numerical simulation, the DW is initialized in one of the configurations shown in the top images of Fig. 2(c) : either an "$n = 1$"sine mode or an "$n = 0$" cosine mode, using once again the numbering of Slonczewski.[29] The DW is then let to relax with no initial velocity. In both cases, its movement is initially highly nonlinear, and then rapidly falls into a damped oscillation of the $n = 1$ mode. Higher orders of the DW are also occasionally observed. The frequency spectrum of the DW elongation obtained by fast Fourier transform is centered around the free-oscillation frequency f_{FO} of the DW. This frequency is found to decrease when the thickness increases: $f_{FO} = 8.20, 2.34, 1.28$, and 0.88 GHz for $h = 10, 20, 30$, and 40 nm, respectively.

Let us now compare these frequencies with the precession frequency of the magnetization within the DW (solid line in Fig. 7, independent of layer thickness). As shown by the arrows in Fig. 7, when the applied field induces a precession frequency close to f_{FO}, a velocity peak is obtained. The v(H) peak and the $\eta_0(H)$ therefore likely correspond to the resonance of the $n = 1$ flexion mode of the DW.

More exactly, the free-oscillation resonance field falls slightly higher than the actual peak for $h = 20$ nm (78 mT instead of $\mu_0 H_{res} = 70$ mT) and 30 nm (48 mT instead of $\mu_0 H_{res} = 35$ mT), and between the peak and the bump for $h = 40$ nm (35 mT). An explanation as to why the peaks are observed at lower frequency than expected from the free-oscillation simulations can be put forward. A DW in movement (under field) cannot be expected to have quite the same resonance frequency as a freely oscillating DW. In particular, applying an external field H_z will be a disadvantage to the higher-order modes of the DW where magnetic charges due to its curvature will create an important magnetostatic contribution. For $H_z = 0$, the free-oscillation frequency likely reflects the presence not only of the $n = 1$ mode but also of higher-order (and higher-frequency) modes. These are indeed observed when plotting the DW depth profile. These higher modes are progressively stifled upon increasing the field, and the frequency spectrum brought lower. This has been verified by doing Fig. 2(c)-type simulations for $h = 20$ nm under an applied field of 1, 3, 7.5, and 15 mT. As a result, the resonance under field appears at a slightly lower frequency
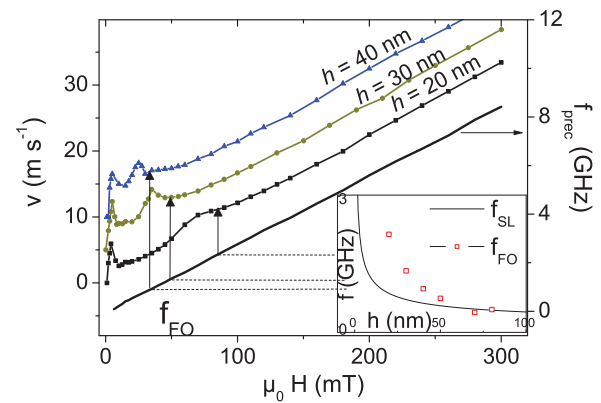

FIG. 7. (Color online) Velocity versus field curves (closed symbols, shifted vertically for clarity), and precession frequency (solid line): the fields giving the peaks in the v(H) curves coincide with the ones yielding the simulated free-oscillation frequencies ($H = 0$). Inset comparison between the thickness dependence of the analytical resonance frequencies (f_{SL}) given in Ref. 29 and the numerically simulated ones (f_{FO}).

(and lower fields) than the free oscillation frequency. An interesting conclusion to this is that a DW cannot truly be considered as a harmonic oscillator as is often argued (Ref. 35 and references therein), but rather as a parametric oscillator whose resonance frequency will effectively depend on the forcing function (applied field in our case).

B. Analytical model

Slonczewski[29] established an approximate expression for the flexural mode frequencies f_{SL} of an assembly of domains arranged in stripes of infinite length (no applied field), neglecting damping. In our 2D geometry (neglecting modes propagating along the wall for now), they can be expressed as a function of n-indexed wave vectors $k_z(n) = n\pi/h$:

$$f_{SL} = \frac{\gamma}{2\pi}\sqrt{\mu_0 M + \frac{2A}{M}k_z^2}\sqrt{\mu_0 M \Delta k_z + \frac{2A}{M}k_z^2}. \quad (12)$$

The inset of Fig. 7 compares the simulated resonance frequencies determined above (f_{FO}, open squares) with the frequency of the first f_{SL} mode computed from Eq. (12) with the numerical simulation's parameters. Since f_{SL} was established at the first order in Δk_z, it largely underestimates the resonance frequencies for very thin layers, but both plots eventually converge for $h > 70$ nm. Using Eq. (12) as a guideline shows that, for $h \gg \Delta$ and $h \geqslant \Lambda$, the position of the peaks in v(H) (given by f_{FO}) will vary roughly like $1/h$ with thickness and be very dependent on the Λ/h ratio. It will not depend on the uniaxial anisotropy. This is to be compared with the $\sqrt{A}$ dependence of the oscillation frequency of a transverse DW simulated numerically in Permalloy.[35] For sample thicknesses much larger than the exchange length, the frequency will vary as $1/\sqrt{h}$, $A^{1/4}$, and $K_u^{-1/4}$. Although Eq. (12) can serve as a general guideline, one must, however, keep in mind that the restoring force in Ref. 29 is somewhat different from the one in our geometry.

VI. DISCUSSION

Let us now consider how the experimental data of Fig. 1 can be explained in the light of the proposed model. Contrary to the virtual material used in the simulations, GaMnAs also exhibits a complex *in-plane* anisotropy, which can induce anisotropic velocities leading to spectacular noncircular domain shapes.[36] However, the difference in velocity along the main axes being around 10% only, the effect of the in-plane anisotropy is likely much weaker than the mechanisms described above.

The simulations [$h = 20$ and 40 nm of Figs. 3(b) and 3(d)] reproduce qualitatively the low-field (region 1) kinks of the corresponding GaMnAs samples, but they do not appear at the same fields. The high-field (region 2) anomalies are not reproduced in the simulations. To estimate where the flexion-induced kinks could be expected for each sample, the DW resonance frequencies were then determined for each $h = 50$ nm sample by micromagnetic simulations ($\mu_0 H = 0$) as described above, using the experimental values of M, K_u, and A.[21] No sufficiently accurate value of A was available for the $h = 20$, 40 nm samples. The resonance fields found by comparing f_{FO} with the precession frequency are indicated by arrows directly on the v(H) curves of Fig. 1(a) and 1(b): 48, 40, and 23 mT for the GaMnAsP sample (T = 20–80 K), and 48.5, 38, 37, 29, and 31 mT for the GaMnAs sample (T = 4–90 K). The arrows point to fields of the same order of magnitude as the ones at which the anomalies are observed. Together with the fact that only the region 1 kinks vary downward with temperature and upward with thickness, region 1 likely corresponds to flexion/twist-induced kinks. A better prediction of the kink shapes and positions would very probably be obtained by doing full 3D simulations, as well as taking into account the influence of additional flexural modes of vibrations (propagating along the plane of the DW and described by a $k_{//}$ wave vector) on the resonance frequency of the DW. The dispersion curves calculated in Ref. 29 (Fig. 6 in particular) seem to suggest that the resonance frequency slightly increases with $k_{//}$. This would likely give a slightly more spread-out feature extending to higher energies.

The region 2 kinks in GaMnAs and GaMnAsP can therefore not be explained by the twist/curvature model, as they shift only weakly with thickness or temperature. A tentative explanation for the origin of these kinks is the parametric excitation put forward by Randoshkin[37] whereby the bulk SWs of the domains couple to the DW magnetization, thus providing an efficient energy dissipation channel, leading to a velocity increase. This phenomenon is expected for frequencies equal to twice the precession frequency: $f_{\text{bulk}} = 2 f_{\text{prec}}$, which would be slightly above region 2 for all samples given their anisotropy fields. The mechanism for this coupling has however never been fully investigated. In the simulations, it would appear at around $H_u/3 = 179$ mT. It has not been observed, possibly due to the strong damping in the simulations.

VII. CONCLUSION

To summarize, we have investigated experimentally and numerically field-driven DW propagation in ferromagnetic layers of thickness close to the exchange length. The data reveal anomalous velocity peaks appearing in the precessional regime, which were partially reproduced numerically. The simulations show that these low-field anomalies are correlated with the maximum flexion of the DW and the maximum twist of the magnetization vector inside the wall, both being intimately coupled. To elucidate their respective roles, we complement the historical (q, ψ) DW propagation model with the phenomenologically determined $\nabla \psi$ (twist). The velocity peaks are then well reproduced and found to result from the torque effect of the stray field on the twisted magnetization. When the DW magnetization is sufficiently twisted across the layer thickness, the stray field emanating from the up- and down-domains surrounding it induces an efficient torque on the total DW magnetization. Because the amplitude of this twist varies over one precession period, the torque averages out to a strictly positive value. Anomalies in v(H) curves are therefore obtained for the particular range of thickness over the exchange length ratio, allowing a strong twist of the DW magnetization, but forbidding the appearance of HBLs, which tend to stifle the velocity enhancement. The resonance field of the twist/curvature is such that the corresponding precession frequency is then close to the DW flexural resonance frequency, and strongly depends on the layer thickness. The experimental v(H) curves obtained for ferromagnetic GaMnAs and GaMnAsP layers show velocity enhancement related to this DW magnetization twist and stray field-induced torque just above Walker breakdown. At a high field, they exhibit broad velocity bumps of different origins, which may be related to nonlinear excitation of bulk SWs not evidenced by our 2D simulations. A full 3D simulation of the velocity would surely yield additional information.

The description of the velocity versus field curve in terms of the ($q,\psi,\nabla q,\nabla \psi$) variables is an alternative and promising way to understand DW propagation experiments in perpendicular-to-plane magnetized samples. The case of Bloch DWs being much simpler in essence than transverse or vortex DW of in-plane magnetized layers, one must be cautious to apply this model to explain the experimental observations of Refs. 12 and 13. Different from our analysis, the work of Yang *et al.*[13] seems to point out that the kinks they observe in v(H) curves without an applied transverse field stem from the stabilization of vortex-antivortex modes, but they have not isolated the physical origin of the appearance of this phenomenon at particular fields. The study of in-plane magnetized layers would therefore call for more thorough investigation, as well as the relevance of our model in current-induced DW propagation experiments.[15]

*e-mail:thevenard@insp.jussieu.fr

[1] N. L. Schryer and L. R. Walker, J. Appl. Phys. **45**, 5406 (1974).

[2] J. C. Slonczewski, J. Appl. Phys. **44**, 1759 (1973).

[3] F. B. Hagedorn, J. Appl. Phys. **45**, 3129 (1974).

[4] A. A. Thiele, J. Appl. Phys. **45**, 377 (1974).

[5] A. Malozemoff and J. Slonczewski, Phys. Rev. Lett. **29**, 952 (1972).

[6] R. P. Cowburn, Patent GB0820844.9, Great-Britain, 12/24/08.

[7] M. Diegel, S. Glathe, R. Mattheis, M. Scherzinger, and E. Halder, IEEE Trans. Magn. **45**, 3792 (2009).

[8] S. S. P. Parkin, M. Hayashi, and L. Thomas, Science **320**, 190 (2008).

[9] P. J. Metaxas, J. P. Jamet, A. Mougin, M. Cormier, J. Ferré, V. Baltz, B. Rodmacq, B. Dieny, and R. L. Stamps, Phys. Rev. Lett. **99**, 217208 (2007).

[10] A. Dourlat, V. Jeudy, A. Lemaître, and C. Gourdon, Phys. Rev. B **78**, 161303 (2008).

[11] G. S. D. Beach, C. Nistor, C. Knutson, M. Tsoi, and J. L. Erskine, Nat. Mater. **4**, 741 (2005).

[12] R. Moriya, M. Hayashi, L. Thomas, C. Rettner, and S. S. P. Parkin, Appl. Phys. Lett. **97**, 142506 (2010).

[13] J. Yang, G. S. D. Beach, C. Knutson, and J. L. Erskine, e-print arXiv:1103.6056 (2011).

[14] G. P. Vella Coleiro, AIP Conf. Proc. **24**, 595 (1975).

[15] M. Hayashi, L. Thomas, C. Rettner, R. Moriya, and S. S. P. Parkin, Nat. Phys. **3**, 21 (2006).

[16] G. Beach, C. Knutson, M. Tsoi, and J. Erskine, J. Magn. Magn. Mater. **310**, 2038 (2007).

[17] A. Thiaville, Y. Nakatani, F. Piéchon, J. Miltat, and T. Ono, Eur. Phys. J. B **60**, 15 (2007).

[18] J.-P. Adam, N. Vernier, J. Ferré, A. Thiaville, V. Jeudy, A. Lemaître, L. Thevenard, and G. Faini, Phys. Rev. B **80**, 193204 (2009).

[19] J. C. Slonczewski, J. Appl. Phys. **45**, 2705 (1974).

[20] G. Patterson, R. Giles, and F. Humphrey, IEEE Trans. Magn. **27**, 5498 (1991).

[21] S. Haghgoo, M. Cubukcu, H. von Bardeleben, L. Thevenard, A. Lemaître, and C. Gourdon, Phys. Rev. B **82**, (2010).

[22] L. Thevenard, L. Largeau, O. Mauguin, A. Lemaître, K. Khazen, and H. J. von Bardeleben, Phys. Rev. B **75**, 195218 (2007).

[23] M. Cubukcu, H. J. von Bardeleben, K. Khazen, J. L. Cantin, O. Mauguin, L. Largeau, and A. Lemaître, Phys. Rev. B **81**, 041202 (2010).

[24] The code is available at [http://math.nist.gov/oommf].

[25] The strip length was long enough to avoid spurious effects arising from magnetic charges at the edges, except for fields 0–10mT for which a nonuniform field was applied in order to compensate for this effect.

[26] C. Gourdon, A. Dourlat, V. Jeudy, K. Khazen, H. J. von Bardeleben, L. Thevenard, and A. Lemaître, Phys. Rev. B **76**, 241301 (2007).

[27] K. Khazen, H. J. von Bardeleben, M. Cubukcu, J. L. Cantin, V. Novak, K. Olejnik, M. Cukr, L. Thevenard, and A. Lemaître, Phys. Rev. B **78**, 195210 (2008).

[28] A. Mougin, M. Cormier, J. P. Adam, P. J. Metaxas, and J. Ferre, Europhys. Lett. **78**, 57007 (2007).

[29] J. Slonczewski, J. Magn. Magn. Mater. **23**, 305 (1981).

[30] A. Hubert, J. Appl. Phys. **46**, 2276 (1975).

[31] A. P. Malozemofff and J. C. Slonczewski, *Magnetic Domain Walls in Bubble Materials* (Academic, New York, 1979).

[32] F. B. Hagedorn and E. M. Gyorgy, J. Appl. Phys. **32**, S282 (1961).

[33] E. Schlömann, Appl. Phys. Lett. **19**, 274 (1971).

[34] M. Farle, Rep. Prog. Phys. **61**, 755 (1998).

[35] J. Rhensius, L. Heyne, D. Backes, S. Krzyk, L. J. Heyderman, L. Joly, F. Nolting, and M. Kläui, Phys. Rev. Lett. **104**, 067201 (2010).

[36] C. Gourdon, V. Jeudy, A. Cebers, A. Dourlat, K. Khazen, and A. Lemaître, Phys. Rev. B **80**, 161202 (2009).

[37] V. V. Randoshkin, Sov. Phys. Solid State **28**, 859 (1986).